A Simulation Framework to Support the Design and Evaluation of Adaptive Scanning for Phased-Array Weather Radars

SEBASTIÁN M. TORRES[a,b] AND DAVID SCHVARTZMAN[a,b]

[a] *Cooperative Institute for Mesoscale Meteorological Studies, University of Oklahoma, Norman, Oklahoma*
[b] *NOAA/OAR/National Severe Storms Laboratory, Norman, Oklahoma*

(Manuscript received 10 June 2020, in final form 12 October 2020)

ABSTRACT: We propose a simulation framework that can be used to design and evaluate the performance of adaptive scanning algorithms on different phased-array weather radar designs. The simulator is proposed as tool to 1) compare the performance of different adaptive scanning algorithms on the same weather event, 2) evaluate the performance of a given adaptive scanning algorithm on several weather events, and 3) evaluate the performance of a given adaptive scanning algorithm on a given weather event using different radar designs. We illustrate the capabilities of the proposed framework to design and evaluate the performance of adaptive algorithms aimed at reducing the update time using adaptive scanning. The example concept of operations is based on a fast low-fidelity surveillance scan and a high-fidelity adaptive scan. The flexibility of the proposed simulation framework is tested using two phased-array-radar designs and three complementary adaptive scanning algorithms: focused observations, beam clustering, and dwell tailoring. Based on a significant weather event observed by an operational NEXRAD radar, our experimental results consist of radar data that were simulated as if the same event had been observed by arbitrary combinations of radar systems and adaptive scanning configurations. Results show that simulated fields of radar data capture the main data-quality impacts from the use of adaptive scanning and can be used to obtain quantitative metrics and for qualitative comparison and evaluation by forecasters. That is, the proposed simulator could provide an effective interface with meteorologists and could support the development of concepts of operations that are based on adaptive scanning to meet the evolutionary observational needs of the U.S. National Weather Service.

KEYWORDS: Algorithms; Radars/Radar observations; Sampling; Weather radar signal processing

1. Introduction

The U.S. National Weather Service (NWS) operates a network of 159 S-band, Doppler, dual-polarization radars (Crum and Alberty 1993) that provide critical real-time data in support of forecasters' warning decision-making processes (Andra et al. 2002). Deployed from 1992 through 1997 and originally designed for a 20-yr service life, this network of Weather Surveillance Radar-1988 Doppler (WSR-88D) instruments was upgraded to dual polarization in the early 2010s [Radar Operations Center (ROC); ROC 2018]. Recently, the WSR-88Ds have undergone a series of comprehensive technological updates that are expected to extend their service life to 2040 (ROC 2020). Beyond this date, it is uncertain whether the WSR-88D will remain viable as one of the most important observing systems for the NWS. Thus, several candidate replacement systems are currently being evaluated to eventually inform a procurement process that may begin around 2030 (NWS 2020).

A fundamental premise in this process is that any candidate replacement radar must meet a set of so-called threshold functional requirements (NWS 2015), which are broadly based on the performance of the WSR-88D (ROC 2007). In addition, the NWS defined a set of optimal (or objective) functional requirements that would result in improved capabilities aimed at supporting its evolutionary weather observing needs. As such, it is expected that preference will be given to candidate radar designs that meet or approach one or more optimal requirements. However, these more capable systems will likely use more radar resources compared to the WSR-88D and result in increased system complexity and/or cost.

In the context of radar design, the fundamental resources can be represented by power-aperture, time, bandwidth, and control-and-processing software (Jeffrey 2009). These resources define nontrivial trade-off spaces involving capabilities, cost, and complexity. For example, as proposed by Zrnić et al. (2015), a requirement for faster radar-data updates could be met by a system operating with simultaneous independent transmit beams at different frequencies to cover the volume scan more quickly. In this case, improved capability in terms of faster updates is achieved by imposing a larger demand on the transmitter bandwidth. Alternatively, the same requirement could be met by a different system operating with reduced dwell times and a higher transmitter power to improve the signal-to-noise ratio (SNR) and thus maintain the overall data quality. In this example, there would be a larger demand on the transmitter power.

One way to reduce the coupling between radar capabilities, cost, and complexity is to recognize that it may not be necessary to meet all functional requirements simultaneously. That is, candidate replacement radars could meet subsets of functional requirements at different times while still supporting the mission needs of the NWS. For example, whereas a sensitivity requirement may be imposed to detect weaker radar returns associated with light precipitation systems or clear air, these

Corresponding author: Sebastián Torres, sebastian.torres@noaa.gov

DOI: 10.1175/JTECH-D-20-0087.1

types of situations may not require a high azimuthal resolution. Conversely, sensitivity may not be a driving requirement to support the observation of strong convective storms, whereas providing a high azimuthal resolution could be important in these situations. Under this paradigm, more demands could be placed on the control-and-processing software to provide forecasters with radar data that support their warning-decision process at a given time. In other words, the radar can give forecasters the data they need when and where they need them. This is the concept of adaptive scanning, which has been explored both using simulations (e.g., Proud et al. 2009; Reinoso-Rondinel et al. 2010; Nguyen and Chandrasekar 2017; Weber et al. 2017; Schvartzman et al. 2017) and through implementations on research and operational radars. While some of the earlier implementations of adaptive scanning were on radar systems with reflector antennas (e.g., Meischner et al. 1997; McLaughlin et al. 2009; Chrisman 2009; Junyent et al. 2010; Daniel et al. 2014; Kollias et al. 2014), the effectiveness of these approaches can be severely limited by mechanical inertia. Conversely, phased-array radars (PAR) that use electronic beam steering provide unique scanning flexibility (Zrnić et al. 2007) and thus the greatest potential for improved capabilities using adaptive scanning (e.g., Heinselman and Torres 2011; Torres et al. 2016). Whereas many of the unique capabilities of PAR can be leveraged to design radar systems that meet all functional requirements simultaneously (e.g., Zrnić et al. 2015), if exploited effectively, adaptive scanning with PAR could result in relatively less complex and/or more cost-effective radar designs.

It is not trivial to develop an adaptive scanning concept of operations (ConOps) that makes efficient use of radar capabilities and still meets NWS mission needs. The first challenge consists of understanding what is essential for forecasters facing different types of weather threats. Unfortunately, our understanding of which functional requirements must be met under different conditions and which ones may be relaxed is limited. For example, in the presence of rapidly evolving convective storms, forecasters may need radar data with faster updates (Heinselman et al. 2008; Brotzge et al. 2010; LaDue et al. 2010; Heinselman et al. 2012; Bowden et al. 2015), though this need may not apply to clear-air regions. The next challenge is to design an algorithm that can adaptively manage the radar resources in order to meet those functional requirements under the specified conditions. Following on the previous example, an effective way to produce radar data for convective storms with faster updates is to focus the rapid scans on volumetric regions with precipitation echoes of interest (Chrisman 2009; Heinselman and Torres 2011). Here, ''interest'' can be defined in different ways depending on the type of weather, the location, spatial extent, and temporal evolution of echoes, and the needs of the forecaster. The final challenge is to define a ConOps for the adaptive scanning algorithm. That is, deciding which information is needed to inform the adaptive decisions and how it will be obtained. For the same example, a fast low-fidelity deterministic scan with full coverage can be used to identify regions with significant weather echoes; in turn, this information can be used to drive the adaptive algorithm to redefine the scan strategy and thus result in focused observations with faster updates (Torres et al. 2016). In general, designing an adaptive scanning ConOps and a radar system that can support it requires an iterative process in which consumers of radar data and radar engineers work collaboratively to identify practical solutions that can provide the needed performance. In this context, realistic simulations are a practical means to conduct a fair evaluation of the performance of different adaptive scanning ConOps on a variety of weather situations using different radar system designs.

The use of simulations to design and/or evaluate the performance of adaptive scanning on weather radars is not new. For example, Proud et al. (2009) used simulations to evaluate adaptive scanning algorithms for Collaborative Adaptive Sensing of the Atmosphere (CASA) radars in terms of their ability to produce radar data that would contribute to the identification of circulations. In that work, the authors focused on analyzing synthetic fields of Doppler velocity from idealized circulations with varying characteristics as observed with different azimuthal resolutions and sampling intervals. More recently, Weber et al. (2017) presented an adaptive scanning algorithm that reduces the update time by leveraging the ability of PARs to use multiple simultaneous receive beams. Their algorithm adaptively determines the size of beam clusters depending on the spatial characteristics of the reflectivity data. As in our work, the authors used archived WSR-88D reflectivity fields. However, they adopted a simplistic simulation approach that does not include all radar variables and does not account for realistic effects such as statistical fluctuations of the weather signal, signal processing effects, beam broadening, antenna pattern sidelobe and cross-polar degradations, or sensitivity changes for different cluster sizes and different beams in each cluster.

In this work, we describe a simulation framework to evaluate the performance of adaptive scanning ConOps on different phased-array radar designs. The simulator produces realistic fields of radar data that could be used to 1) compare the performance of different adaptive scanning ConOps on the same weather event, 2) evaluate the performance of a given adaptive scanning ConOps on several weather events, or 3) evaluate the performance of a given adaptive scanning ConOps on a given weather event using different radar designs. In other words, the simulated radar data produced by the proposed simulation framework can serve as a ''common language'' between engineers and meteorologists, allowing the development and evaluation of feasible ConOps to meet evolutionary NWS observing needs. The rest of the paper is organized as follows. Section 2 describes the simulation framework, which allows the implementation and evaluation of a wide variety of adaptive scanning ConOps targeting one or more of forecaster needs (e.g., update-time reduction, larger spatial coverage, finer spatial sampling, or improved radar data quality). Section 3 presents a particular instantiation of this framework to demonstrate the use of adaptive scanning as a means to reduce the update time. Section 4 illustrates how the simulation framework can be used to design and evaluate different adaptive scanning ConOps and to compare their performance on different radar designs. The conclusions and proposed future work are summarized in section 5.

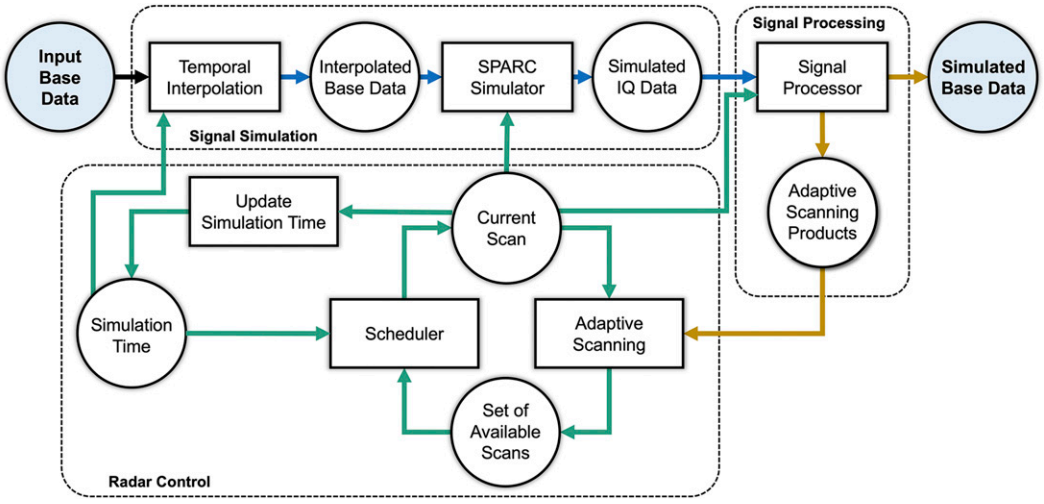

FIG. 1. Block diagram of the proposed simulation framework consisting of three subsystems: signal simulation, signal processing, and radar control. Input base data are used to produce simulated base data as would be observed with a user-defined radar system and adaptive scanning ConOps.

2. Simulation framework

The simulation framework described in this section is proposed as a unique means to design and evaluate the performance of different adaptive scanning ConOps using realistic fields of radar data. Moreover, simulations enable the comparison of different ConOps and different radar designs in meaningful ways since the same weather event can be used for all ConOps and radar combinations. Thus, the effects of different radar designs and their associated (potentially different) ConOps on the quality of the radar data can be assessed using true apples-to-apples comparisons, which could not be done with real radar systems or with simplistic emulations. In other words, the proposed simulation framework provides the best of both worlds: realistic radar data corresponding to the use of different radars and different ConOps, and the ability to reprocess the same weather event in different ways.

Figure 1 shows a block diagram of the proposed simulation framework comprising three subsystems: signal simulation, signal processing, and radar control. At a high level, a typical adaptive scanning ConOps simulation involves the execution of several simulation cycles, where a simulation cycle is defined by the execution of a volume scan (herein referred to simply as a scan). At the beginning of a simulation cycle, the simulation time is updated by adding the previous scan time. That is, the simulation time corresponds to the beginning of a simulation cycle and advances at discrete and generally irregular time intervals. For the next step in the simulation cycle, a scheduler selects the current scan out of a set of available scans by following the particular rules of the adaptive scanning ConOps. With that information, the signal simulation subsystem produces realistic time series [in-phase and quadrature (IQ)] signals that include the combined effects of the radar system characteristics and the acquisition parameters of the current scan. The signal processor subsystem ingests these IQ signals and, depending on the scan purpose, may produce conventional radar variables (the outputs of the simulator) and/or adaptive scanning products (internal to the simulator). If the current scan produces adaptive scanning products, these are used by the adaptive scanning algorithms to modify one or more scans, which may include the current scan. This cycle repeats until the desired simulation time period is completed. Next, we describe the main components of the simulation framework and each subsystem in more detail.

a. Radar definition

As mentioned before, the simulation framework allows the emulation of different radar systems. A radar system is specified through a set of relevant parameters that describe its main design characteristics and how they relate to the radar system used to collect the input data (herein referred to as the reference radar). One of the main design characteristics in the radar definition is the antenna type. In our current implementation, the antenna type can be a mechanically scanned reflector, a mechanically and electronically scanned single-face planar phased array, an electronically scanned four-face planar phased array, or an electronically scanned cylindrical phased array. For these radars, the antenna aperture size is indirectly specified by the 3-dB one-way effective antenna radiation pattern. For a PAR system, this is the pattern used for narrow (pencil) beam operation corresponding to a full nontapered aperture transmission. Any radar beamforming capabilities are implied in the transmit and receive antenna radiation patterns that can be selected (adaptively or not) in the simulation. Another important design characteristic is the radar sensitivity. The radar definition includes a sensitivity factor that is defined by the sensitivity of the longest waveform relative to that of the reference radar. This parameter includes differences in transmitter peak power, narrow-beam antenna gain, system losses, and receiver noise power. It is important to note that the

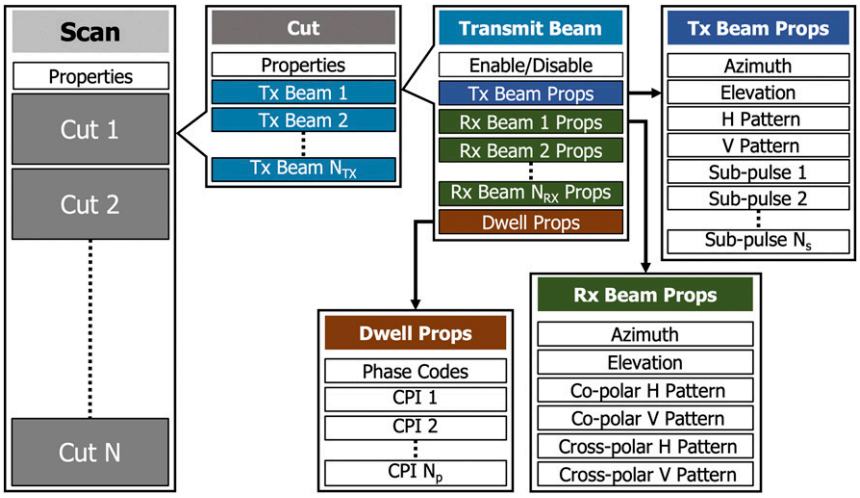

FIG. 2. Representation of the scan definition used by the proposed simulation framework.

simulation can only handle sensitivity factors equal to or less than 1. That is, the resulting sensitivity of the emulated radar cannot exceed that of the reference radar. The transmission bandwidth is implied in the waveforms that can be selected (adaptively or not) in the simulation. Because we are not trying to compare radars in different frequency bands or to study the frequency-dependent scattering differences between radar systems, an implicit assumption is that the frequency of the simulated radar matches that of the reference radar.

b. *Scan definition*

The scan is the fundamental simulation unit. Its definition contains all necessary information to control different aspects of radar transmission, reception, and signal processing. Figure 2 shows a schematic representation of the scan structure. At a high level, a scan is a set of transmit beams organized as a collection of constant-elevation cuts (hereafter simply referred to as cuts). The main properties of a scan are the azimuthal sampling scheme (degree space for rotating antennas and either sine or degree space for stationary phased-array antennas), the azimuth of broadside with respect to north for stationary antennas, and the total azimuthal coverage (0°–360°). Each cut contains an ordered list of transmit beams and cut-specific properties, which include the transmit and receive azimuthal sampling spacings. Note that for radar systems with no advanced beamforming capabilities (e.g., those based on reflector antennas or passive phased-array antennas), the transmit and receive azimuthal sampling spacings are the same. That is, there is only one receive beam for each transmit beam. However, for radar systems with advanced beamformers, there could be more than one receive beam for each transmit beam. This is typically referred to as imaging or beam spoiling and involves the use of broader or multilobe transmit beam patterns. Note that, in this work, broad or multilobe transmit beams are also referred to as transmit beams.

Each transmit beam in the scan corresponds to a dwell from which one or more radials (or rays) of radar-variable estimates will be generated by the signal processor. A radial contains radar data for all range locations in a given azimuth–elevation direction. A transmit beam can be either scheduled (enabled) in the scan or not scheduled (disabled) and is specified by transmit, receive, and dwell properties. The transmit properties contain the transmit beam boresight azimuth and elevation, the transmit antenna radiation patterns for each polarization, and the transmit pulse. The transmit pulse can be specified as a sequence of one or more independent base-band transmission waveforms, also referred to as subpulses; the assumption here is that these subpulses are transmitted on different frequency subbands and the waveforms can employ arbitrary modulation schemes [e.g., continuous wave, linear frequency modulation, or nonlinear frequency modulation (NLFM)]. For each transmit beam, there can be one or more receive beams. The properties for each receive beam contain the boresight azimuth and elevation and a set of copolar and, for a dual-polarization radar, cross-polar receive patterns. The dwell properties include an optional pulse-to-pulse phase-coding sequence (e.g., Sachidananda and Zrnić 1999; Ivić and Doviak 2016) and definitions for one or more coherent processing intervals (CPI), where each CPI is specified by a pulse repetition time (PRT) and a pulse count.

c. *Signal simulation*

The signal simulation subsystem takes existing radar data (collected by the reference radar) and produces simulated IQ signals using the acquisition and sampling parameters of an arbitrary radar-system and scan definitions. Here, radar data refers to fields of base data (i.e., reflectivity, Doppler velocity, spectrum width for a single-polarization radar and these plus differential reflectivity, differential phase, and correlation coefficient for a dual-polarization radar). For our work, we use archived WSR-88D base data from the National Centers for Environmental Information (NCEI; https://www.ncei.noaa.gov/) because they are easily accessible, they include a large variety of weather scenarios, their spatial domain and temporal sampling (~5 min) are adequate for our simulation needs, and they lead to simulated data with sufficient realism for the intended

purposes. However, the simulator could use fields of base data collected by other radar systems or even outputs of numerical weather prediction models (assuming adequate domain size and diversity of weather scenarios).

The first step in the signal simulation process is the temporal interpolation of the input base data. This is needed to remove the dependency of the simulation time on the temporal sampling of the input data. That is, the simulation scan times do not need to match the update time of the input data. The temporal interpolation function takes the two nearest sets of input data in time (one prior and one after the simulation time) to generate realistic fields of radar variables at arbitrary times. We use the algorithm by Meyer et al. (2015) on every cut in native polar coordinates. This algorithm was developed for video frame interpolation and is computationally simpler than conventional optical-flow methods. In general, the realism of interpolated fields is a function of the time between observations of the reference radar and the degree of storm evolution in this time. For the cases we analyzed, the ~5-min update times of the WSR-88D data are sufficient even for fast-evolving weather phenomena such as tornadic storms. However, it should be noted that the fields of radar data produced in this manner are not meant to be a substitute for data collected with faster updates nor are they meant to reproduce the actual radar-data fields at the interpolation time. Still, they are realistic enough for evaluating the most significant data-quality impacts of different combinations of adaptive scanning ConOps and radar design.

The second step uses the time-interpolated fields of radar data as inputs to the Signal Processing And Radar Characteristics (SPARC) simulator (Schvartzman and Curtis 2019) to produce dual-polarimetric IQ data as determined by the scan definition and radar properties defined above. At a high level, the SPARC simulator takes one volume of base data from the reference radar and first performs a data-conditioning step to fill in any missing data and dealias the velocity fields. Then, it resamples the conditioned fields to match the sampling grids of the antenna radiation patterns and range weighting functions of the emulated radar. For this work, we assume that the scans used in the simulation have the same elevation cuts as the scan used by the reference radar. We also assume that any adaptive scanning algorithms operate in a single cut at a time and do not change the antenna pattern in the elevation dimension. These assumptions are not required by the simulation framework, but greatly reduce the computational complexity of IQ simulations without limiting our ability to demonstrate the proposed concept. If changes in the elevation dimension were expected from the chosen ConOps, the SPARC simulator extension developed by Nai et al. (2020) could be used to perform a volumetric resampling of conditioned fields.

Next, resampled fields of base data are used to simulate IQ data (Curtis 2018) at each point in a fine grid. As the final step, the IQ data are weighted to incorporate the two-way antenna-pattern (which may be different for each beam) and range-weighting-function effects, and the results are spatially decimated in azimuth and range to match the sampling grid of the emulated radar. It is important to note that, for each transmit beam in the scan, the SPARC simulator generates independent dual-polarimetric IQ datasets for each CPI, each frequency subband, and each receive beam. Thus, each IQ dataset can have its own PRT, number of samples, range weighting function, and two-way co- and cross-polarization antenna patterns, allowing the simulation of radar data as if they were collected with a variety of radar systems and scanning strategies. In addition, each IQ dataset can have its own SNR to emulate sensitivity differences arising from a particular combination of radar design and scan definition. Finally, it should be noted that the SPARC simulator does not attempt to recreate the IQ data from the reference radar. Instead, it simulates IQ data that, after signal processing, results in similar depiction of weather features. In other words, the SPARC simulator produces radar data with enough realism such that experts presented with original and simulated fields are unable to determine which one is which (Boettcher and Nai 2020).

d. *Signal processing*

The signal processor ingests simulated dual-polarimetric IQ data for a single receive beam and, depending on the scan purpose, may produce a radial of base data. Recall that each receive beam contains IQ data for all the CPIs and frequency subbands defined in the scan. The signal processing subsystem includes modules for pulsed interference suppression, noise-power estimation (Ivić et al. 2013), ground clutter detection and filtering (Torres and Warde 2014), radar-variable estimation (Doviak and Zrnić 1993), range unfolding and/or velocity dealiasing [if using multi-pulse-repetition-frequency (PRF) dwells], data merging (if using multiple frequency subbands), and data thresholding (e.g., based on the SNR). The base data produced by the signal processor are archived in simulation time using the standard NEXRAD base-data format and can be displayed using conventional data-visualization tools that support this format (e.g., GRLevel2 or the NOAA Weather and Climate toolkit). Depending on the scan purpose, the signal processor may also produce adaptive scanning products, which are the observables derived from the data to be used as inputs to the adaptive scanning algorithms. Depending on the adaptive scanning algorithm, these may include spatial or temporal characteristics of the radar returns such as the minimum and maximum range of significant echoes in a given direction or the expected advection and growth of different storm clusters.

e. *Radar control*

The radar control subsystem includes adaptive scanning and scheduling algorithms that close the simulation loop. To allow for the implementation of a wide range of adaptive scanning and scheduling algorithms, the radar control subsystem is connected to the rest of the simulation framework by generic interfaces: its inputs are adaptive scanning products obtained at the signal processor, and its output is the current scan definition containing any changes imposed by the adaptive scanning algorithms. For each available scan, the scheduler defines a purpose that is used to determine how the IQ data will be processed, whether base data are produced and archived, which adaptive scan products are produced (if any), and which scans may be updated by the adaptive scanning algorithms

TABLE 1. Main characteristics of the two scans used in the adaptive scanning ConOps.

	Coverage	Dwell times	Data quality	Adaptive scanning products	Base data products	Adaptive
Surveillance scan	Full	Short	Poor	Yes	No	No
Adaptive scan	Focused	Nominal	High	No	Yes	Yes

(if any). At the beginning of each simulation cycle, the scheduler determines the next scan out of the set of available scans. The scheduling criteria can be as simple as round-robin scheduling or can be designed to meet specific objectives. An example of the latter is the time-balance algorithm, which can be used to minimize the delay in the execution of multiple scans with individual update-time requirements (Reinoso-Rondinel et al. 2010). The proposed simulation framework provides the proper interface so that a variety of scheduling techniques can be implemented and evaluated. At the end of each simulation cycle, the adaptive scanning algorithms use adaptive scanning products to modify one or more scans in response to observations of the scene with the goal of meeting specific needs. The adaptive scanning algorithm defines which scan parameters are to be modified and how this modification is performed. For example, the algorithm described by Heinselman and Torres (2011) to reduce update times while preserving spatial sampling and data quality uses a radial significance product to modify a scan by disabling transmit beams from locations that do not contain significant weather returns [more on this algorithm is given in section 3b(1)].

In general, the scheduler and adaptive scanning algorithms could change dynamically given that the observational needs may depend on the weather event and/or the needs of forecasters. Responding to these needs could result in changes to the scans in terms of their update time, spatial sampling, and/or associated data quality. For example, the observation of a supercell capable of producing a tornado would require faster updates with the best possible spatial sampling and data quality. However, it may be challenging to meet these competing requirements simultaneously. The ultimate goal of an adaptive scanning algorithm is to produce scans with optimized tradeoffs for each situation, and the proposed simulation framework provides a unique tool to design and evaluate the performance of these algorithms.

3. An adaptive scanning ConOps using the proposed simulation framework

In this section, we describe a particular instantiation of the simulation framework to demonstrate how it can be used as a tool to evaluate an adaptive scanning ConOps that uses three different adaptive scanning algorithms with the common goal of reducing the data update time. To illustrate the flexibility of the proposed simulation framework, we adopt a radar system with four electronically scanned, planar, phased-array antennas. The ConOps uses a fast surveillance scan to modify an adaptive scan as in Torres et al. (2016). This is a simple but effective adaptive scanning ConOps that serves to demonstrate the flexibility and many of the features of the proposed simulation framework. The details of the ConOps and the three adaptive scanning algorithms are presented next.

a. *Concept of operations*

The ConOps under analysis uses two scans: a surveillance (low fidelity) scan and an adaptive (high fidelity) scan. The surveillance scan provides the inputs (i.e., the adaptive scanning products) to the adaptive scanning algorithms, which modify the adaptive scan. The surveillance scan is invariant (i.e., nonadaptive) and uses short dwell times to minimize its scan time while providing full spatial coverage. The base data obtained with the surveillance scan do not meet the requirements for data quality and are only meant to be used internally to produce adaptive scanning products. As such, when processing data from the surveillance scan, the signal processor is configured to produce radar variables using a minimal subset of processing modules that is enough to generate adequate adaptive scanning products.

The adaptive scan is intended to provide the users with base data that meet observational needs. The adaptive scanning algorithms use the adaptive scanning products derived from the surveillance scan to update the adaptive scan in different ways. The base data from the adaptive scan are outputs of the simulator that could be interrogated by forecasters or used as inputs to algorithms; in this implementation, no adaptive scanning products are derived from it. Table 1 summarizes the main characteristics of the two scans in this ConOps; internally, these scans are represented as depicted in Fig. 2 and make up the "set of available scans" in the block diagram of Fig. 1.

The scheduler uses a variant of round-robin scheduling in which the execution of each scan is controlled by a scan-specific repeat counter and/or timer. If using a repeat counter, the scheduler executes the given scan the specified number of times before changing the scan. If using a timer, the scheduler repeats the execution of the given scan until the sum of the scan times exceeds the timer. If using both, the scheduler changes the scan when both conditions are met. This functionality corresponds to the "scheduler" block in Fig. 1.

b. *Adaptive scanning algorithms*

In our example, the adaptive scanning algorithms are designed to reduce the update time of the output base data, which, in this ConOps, is a function of the surveillance and adaptive scan times and the scheduler parameters. Because the surveillance scan does not change, any reduction in the update time can only be realized through a reduction in the adaptive scan time. In general, the scan time is determined by the total number of transmit beams in the scan and their corresponding dwell times. Thus, the scan time can be reduced by reducing the number of transmit beams, by reducing the dwell times, or by a combination of both. In every case, reducing the adaptive scan

TABLE 2. Main characteristics of the lowest-elevation cuts in the surveillance and adaptive scans.

	Surveillance scan	Adaptive scan
Azimuthal sampling spacing	1 beamwidth	0.5 beamwidth
Range sampling spacing	250 m	250 m
Transmission mode	Simultaneous horizontal and vertical polarizations	Simultaneous horizontal and vertical polarizations
Subpulses	80-μs modulated (NLFM) and 1.6-μs unmodulated	80-μs modulated (NLFM) and 1.6-μs unmodulated
Beamforming	Pencil beam	Pencil beam (if the adaptive beam clustering algorithm is not used); pencil beam, spoiled beam by a factor of 3, or spoiled beam by a factor of 5 (if the adaptive beam clustering algorithm is used)
Dwell type	Uniform PRF	Triple PRF (if the adaptive dwell type algorithm is not used); uniform PRF, dual PRF, or triple PRF (if the adaptive dwell type algorithm is used)
Max unambiguous range	450 km	450 km (if the adaptive dwell type algorithm is not used); 150–450 km (if the adaptive dwell type algorithm is used)
Max unambiguous velocity	8.8 m s^{-1}	26.2 m s^{-1}
Dwell time	12 ms	78.5 ms (if the adaptive dwell type algorithm is not used); 20–78.5 ms (if the adaptive dwell type algorithm is used)
Benchmark std dev of reflectivity (SNR = 10 dB; σ_V = 4 m s^{-1})	2.02 dB	1.29 dB (if the adaptive dwell type algorithm is not used); 1.22–1.29 dB (if the adaptive dwell type algorithm is used)

time involves one or more degradations in terms of spatial sampling (resolution and/or coverage), data quality (sensitivity and/or bias and variance of radar-variable estimates), or both. Thus, the update-time reduction is a function of the weather scenario and the adaptive scanning algorithm as will be described later in this section and will be demonstrated in section 4.

Several techniques have been proposed to reduce the update time on PARs (e.g., Lai et al. 2004; Yu et al. 2007; Weber et al. 2007; Heinselman and Torres 2011; Isom et al. 2013; Melnikov et al. 2015; Zrnić et al. 2015; Torres et al. 2016; Weber et al. 2017; Schvartzman et al. 2017). In the context of the four-face PAR adopted here, we select three complementary adaptive scanning algorithms that can be used (individually or in combination) to provide significant update-time reductions: focused observations, beam clustering, and dwell tailoring; these correspond to the "adaptive scanning" block in Fig. 1. While this selection is not arbitrary, it should not be interpreted as suggesting that these algorithms are the only ones or the best ones available to reduce the scan time through adaptive scanning. In other words, the adaptive scanning algorithms presented next are chosen only to illustrate the flexibility of the simulation framework and the realism of the data produced by it. For each algorithm, we provide an assessment of the expected impacts to the quality of radar data and confirm our expectations through experimental results in section 4.

1) FOCUSED OBSERVATIONS (ADAPTS)

The Adaptive Digital Signal-Processing Algorithm for PAR Timely Scans (ADAPTS) algorithm (Heinselman and Torres 2011) exploits the PAR beam agility to only scan regions with significant weather returns. The algorithm adaptively enables or disables transmit beams in the adaptive scan based on echo significance measured from the surveillance scan. Thus, the time savings afforded by ADAPTS depends on the spatial coverage of precipitation systems. The smaller the coverage, the larger the time savings. In this algorithm, a beam position is deemed intrinsically significant if there are sufficient range gates with reflectivity exceeding a user-defined threshold. To account for storm growth and advection, significance is also assigned to beam positions in a predefined spatial neighborhood of beams with intrinsic significance. Our implementation uses a coverage threshold of four consecutive range gates or enough gates to cover a 1-km^2 area (whichever number is larger), a reflectivity threshold of 11 dB, and a neighborhood of two beam positions on either side of each intrinsically significant beam (along the azimuthal direction).

Because ADAPTS only enables or disables transmit beams in the scan, it does not impact the quality of the radar data that it produces. That is, the data from enabled transmit beams in the adaptive scan have the same quality as if they had been obtained without adaptive scanning. However, ADAPTS leads to a deliberate loss of coverage: the resulting fields of radar data exhibit coverage gaps corresponding to the disabled transmit beams.

2) BEAM CLUSTERING

The adaptive beam clustering algorithm exploits the PAR beamforming capabilities to reduce the scan time by simultaneously producing multiple receive beams within a "spoiled" or wider transmit beam (Weber et al. 2017). The time savings afforded by this algorithm is proportional to the spoil factor, where the spoil factor is defined as the width of the spoiled transmit beam with respect to the narrow or pencil beam. However, spoiling the transmit beam comes at a cost: reduced sensitivity and degraded spatial resolution. The former is the result of the transmit power being spread over a larger region of space (i.e., the larger the spoil factor is, the smaller will be

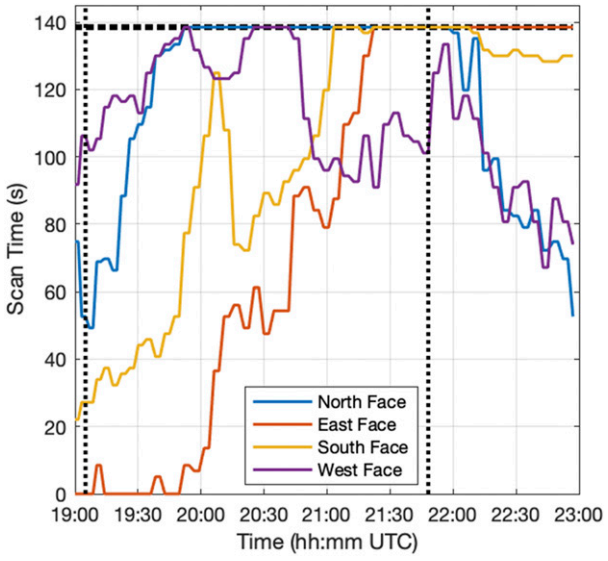

FIG. 3. Scan time for each of the four faces of the full-size radar as a function of simulation time for experiment 2 (using the ADAPTS algorithm). The vertical black dotted lines correspond to time A and time B. The horizontal black dotted line corresponds to the scan time for experiment 1 (using the conventional ConOps).

the transmit antenna gain). The latter is the result of combining a wider transmit pattern with a narrow receive pattern (as opposed to using narrow patterns on both transmit and receive) leading to higher two-way antenna pattern sidelobes and a larger main-lobe width.

To account for these tradeoffs, we devised a requirement-driven adaptive beam clustering algorithm whereby the azimuthal transmit-beam spoil factor is selected based on the spatial structure of the reflectivity data. Unlike the algorithm proposed by Weber et al. (2017) that forces a number of beam clusters to achieve a required scan time, our algorithm creates as many beam clusters as possible while preventing sidelobe contamination from significantly degrading the quality of the data. That is, the use of larger azimuthal beam spoil factors is limited by the presence of large reflectivity gradients in the azimuthal direction (we do not consider spoiling in elevation here). Thus, the smaller the azimuthal gradients of reflectivity, the larger the time savings. The algorithm uses the surveillance-scan reflectivity data to estimate the relative biases that would be incurred through the use of different transmit beam spoil factors. This is done by applying two-way antenna patterns obtained from progressively larger transmit beam spoil factors to the reflectivity field from the surveillance scan. The resulting reflectivity data are compared to the input surveillance data, and relative reflectivity biases are obtained for each range gate. Since the same two-way antenna pattern is used for all range gates in a radial, we use the median of the top-1% biases as a representative metric that captures the worst-case-scenario biases in a robust manner. Using this metric, the algorithm chooses the largest transmit beam spoil factor such that the reflectivity biases resulting from the degraded spatial resolution do not exceed a required threshold (2 dB in our case).

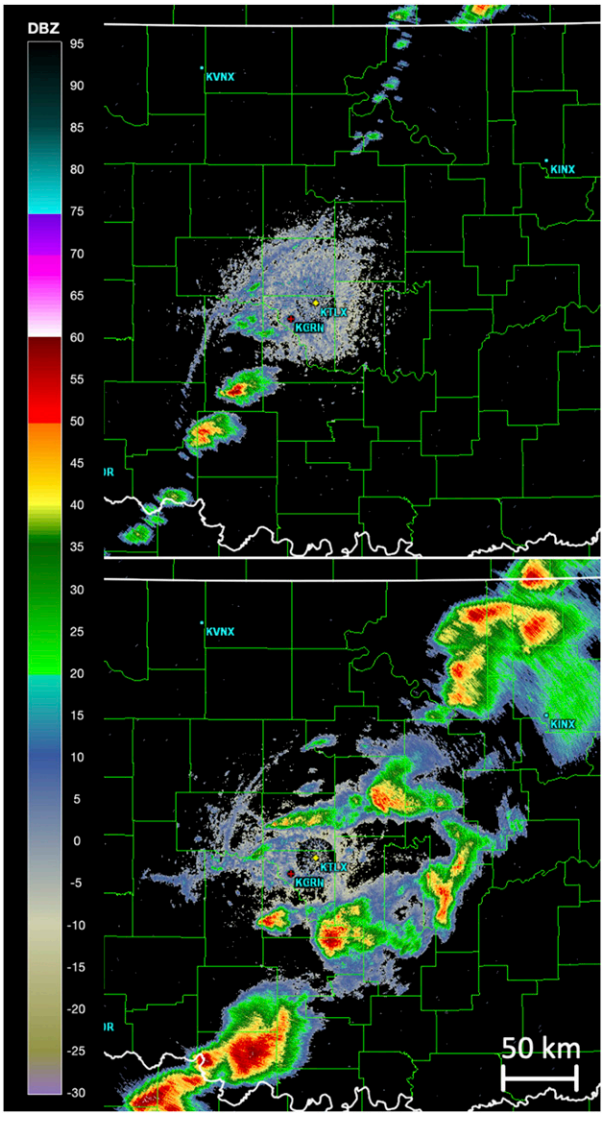

FIG. 4. Fields of reflectivity for the lowest elevation cut (0.5°) for experiment 1 (using the conventional ConOps) for (top) Time A (1905 UTC) and (bottom) time B (2149 UTC).

Once an appropriate spoil factor is determined for a transmit beam, the adaptive scan is modified to use the corresponding transmit pattern and adjacent transmit beams covered by the newly formed cluster of receive beams are disabled. For our implementation, we allow transmit beam spoil factors of 3 and 5, in addition to the conventional narrow pencil beams (i.e., no transmit beam spoiling). For simplicity and as a means to illustrate the flexibility of the simulation framework, this implementation only explicitly considers the quality of reflectivity data, but the algorithm could be generalized to take into account the quality of the other radar variables as well.

Depending on the spoil factor, the adaptive beam clustering algorithm introduces a few impacts to the quality of the radar data. As mentioned before, the larger the spoil factor, the lower the sensitivity and the coarser the spatial resolution

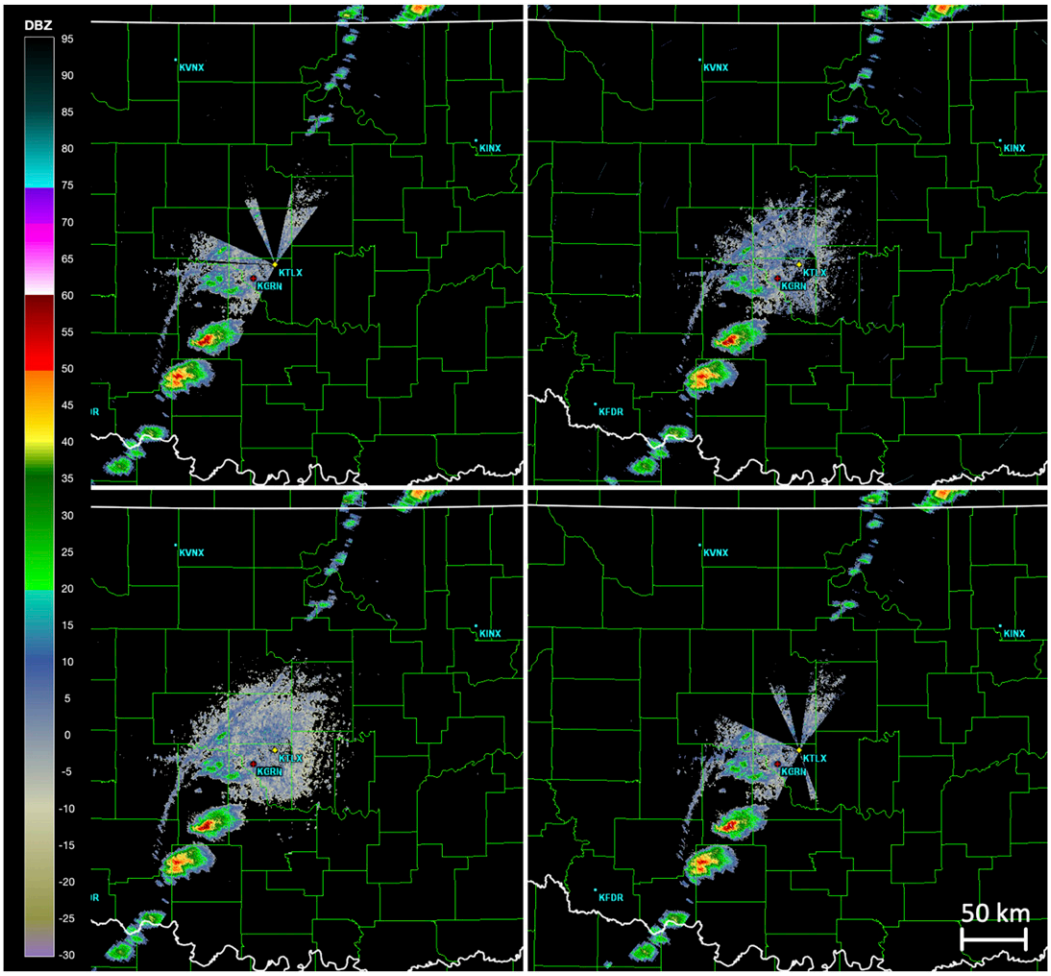

FIG. 5. Fields of reflectivity for the lowest elevation cut (0.5°) at time A for (top left) experiment 2 (using the ADAPTS algorithm), (top right) experiment 3 (using the adaptive beam cluster algorithm), (bottom left) experiment 4 (using the adaptive dwell tailoring algorithm), and (bottom right) experiment 5 (using the three adaptive scanning algorithms concurrently).

(given by a wider antenna pattern main-lobe width and elevated sidelobe levels). Sensitivity changes from the use of different spoil factors are seen in the fields of radar data as abrupt increases or decreases in the footprint of storms or clear-air returns close to the radar. Degradations in the spatial resolution should be seen as positive biases on reflectivity fields, especially in the presence of azimuthal reflectivity gradients. However, the adaptive beam clustering algorithm is designed to limit these biases to 2 dB for over 99% of the gates, so these biases should not be apparent through visual inspection.

3) DWELL TAILORING

The adaptive dwell tailoring algorithm reduces the scan time by using the shortest dwell without compromising coverage or data quality. In our case, multi-CPI (or multi-PRF) dwells, where each CPI employs a different PRF, are used to simultaneously achieve the required spatial coverage and maximum unambiguous velocity. Unfortunately, this comes at the price of longer dwell times. However, when storms are located within the maximum unambiguous range of the shorter PRTs, the number of CPIs can be reduced without impacting the spatial coverage or the data quality. The time savings afforded by the adaptive dwell tailoring algorithm depends on the location of precipitation systems with respect to the radar. The closer the storms are to the radar, the larger the time savings.

In this algorithm, the dwell is tailored to the maximum range of storms, which is determined from the surveillance scan using similar significance criteria as in the ADAPTS algorithm. In this context, tailoring consists of choosing the appropriate CPI subset (from a set of three predetermined CPIs, herein referred to as the high-, medium-, and low-PRF CPIs) and adjusting the total number of samples (also from a set of three predetermined values, one for each CPI). To preserve the maximum unambiguous velocity and reduce the occurrence of velocity aliasing, the CPI with the high PRF is always included.

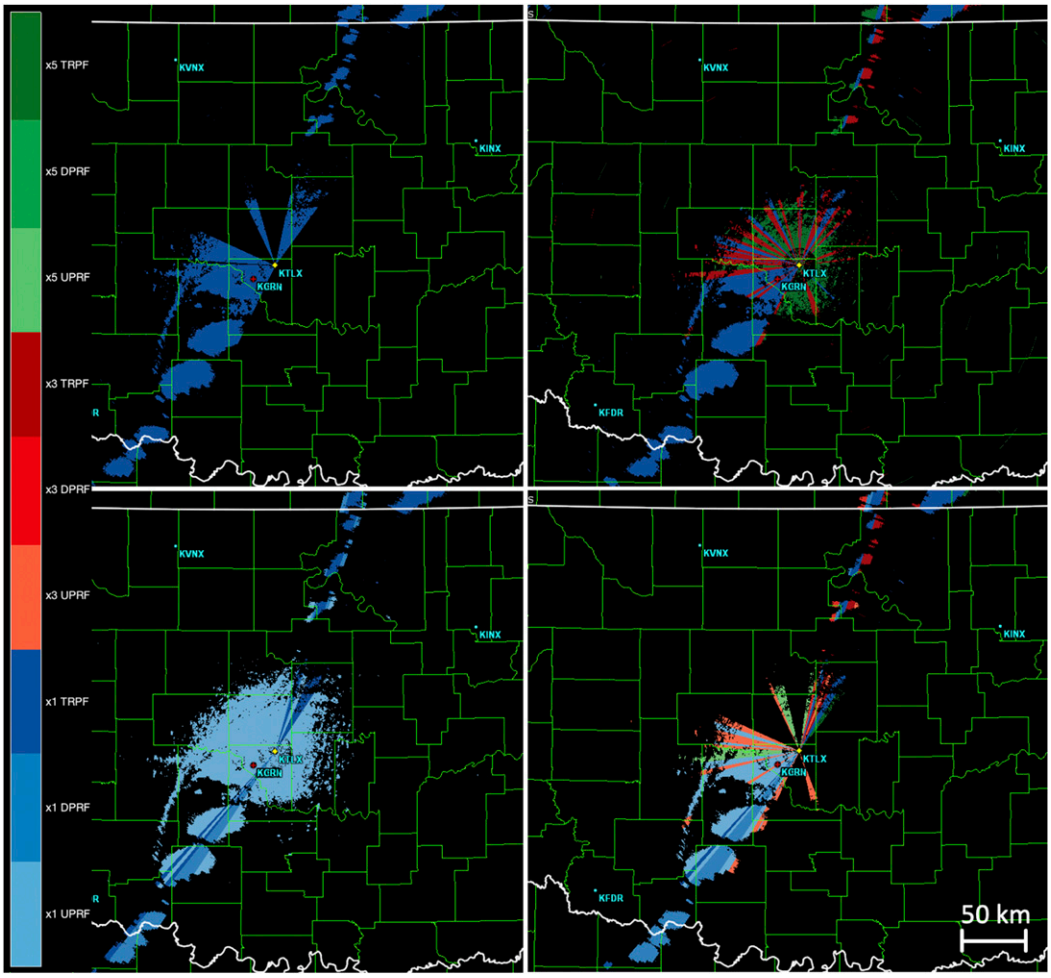

FIG. 6. As in Fig. 5, but for the adaptive scanning products. Transmit beams disabled by ADAPTS are not painted. Pencil beams (×1) are painted in three shades of blue, spoiled beams with a factor of 3 (×3) are painted in three shades of red, and spoiled beams with a factor of 5 (×5) are painted in three shades of green. Transmit beams with single- or uniform-PRF (UPRT) dwells are painted in a light shade of the color corresponding to the spoiling factor, those with dual-PRF (DPRF) dwells are painted in a medium shade, and those with triple-PRF (TPRF) dwells are painted in a dark shade.

That is, when the maximum range of storms is within the maximum unambiguous range of the high PRF, only the CPI with the high PRF is used. However, when the maximum range of storms is between the maximum unambiguous ranges of the high and medium PRFs, the CPIs with the high and medium PRFs are kept. Otherwise, if the maximum range of storms exceeds the maximum unambiguous range of the medium PRF, all CPIs are retained. To preserve data quality, the number of samples of the retained CPI with the lowest PRF is increased (if needed) to match the duration of the longest discarded CPI.

The adaptive dwell tailoring algorithm does not have any apparent impacts to the quality of the radar data. As the number of PRFs is reduced, so is the maximum unambiguous range, but the algorithm is designed to make these changes only in areas where such reduction would not result in reduced coverage. In addition, the dwell tailoring rules are designed to preserve the maximum unambiguous velocity and to adjust the dwell times so that the data quality is not changed with respect to that from the original scan.

4. Experimental results

In this section, we show how the simulation framework can be used to design and evaluate adaptive scanning algorithms and to compare their performance on different PAR designs. We consider two related notional radar designs as in Cho (2015) based on the four-face, electronically scanned, PAR architecture. The first radar is referred to as the ''full size'' PAR. This is a system with a power-aperture similar to that of the WSR-88D. That is, each antenna (or face) has an 8-m-diameter circular aperture with about 10 000 30-W radiating elements per face, resulting in an intrinsic beamwidth at broadside of 1° and a long-pulse sensitivity of −10 dBZ at

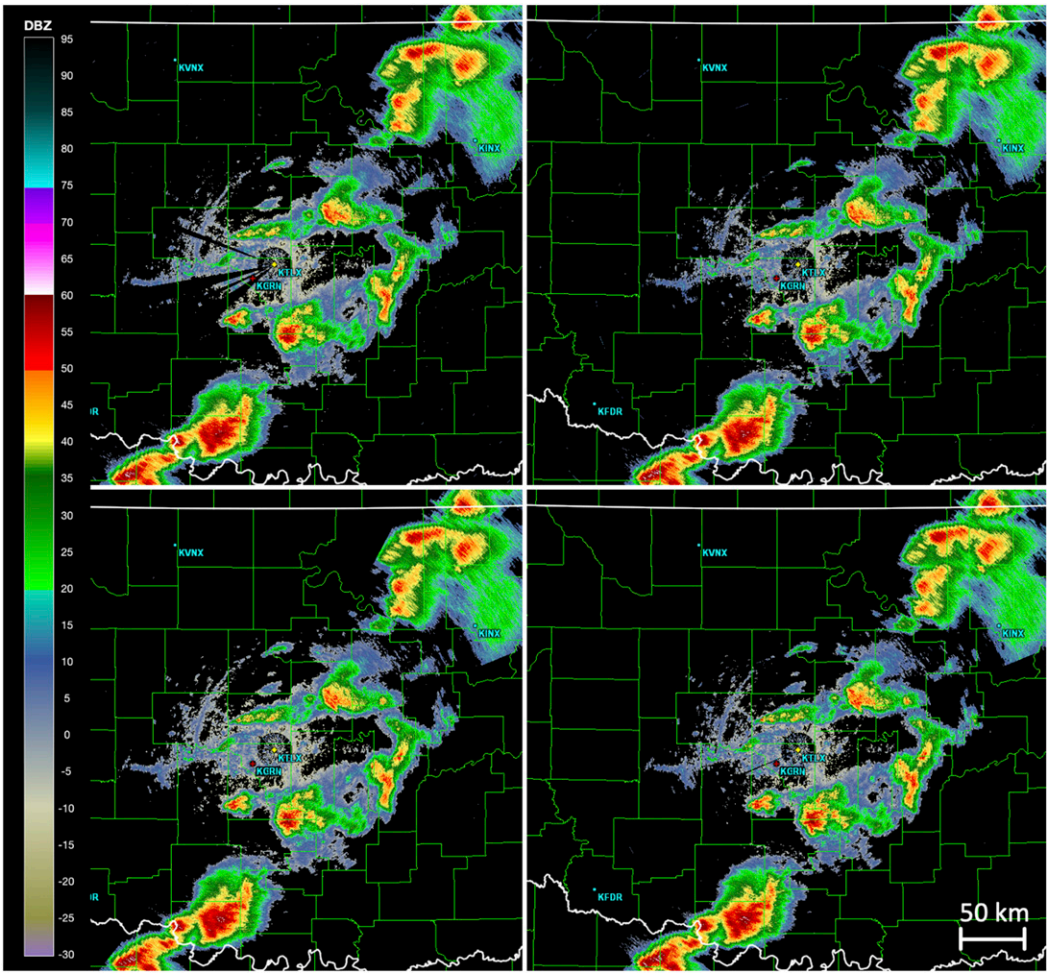

FIG. 7. As in Fig. 5, but at time B.

50 km. The second radar is referred to as the ''terminal-size'' PAR. This system is a scaled-down version of the first radar, it has a power-aperture similar to that of the Airport Surveillance Radar (ASR) and could be used as a gap-filling radar. In this system, each antenna has a 4-m-diameter circular aperture with about 2800 5-W radiating elements per face, resulting in an intrinsic beamwidth at broadside of 2° and a long-pulse sensitivity of -2.5 dBZ at 50 km. Whereas they differ in size and transmit power, the assumption is that both radar systems are based on similar building blocks and have the following common characteristics. The broadsides for the four faces are 0.5° elevation and 0°, 90°, 180°, and 270° azimuth with respect to north; each face covers a 90° azimuthal sector, and they are referred to as the north, east, south, and west faces. Both radars use pulse compression to achieve the desired sensitivity while maintaining a range resolution of 250 m. Available waveforms use a 6-MHz transmission bandwidth and span pulse widths from 38 to 80 μs. A short 1.6-μs unmodulated fill pulse (in a different frequency subband) is transmitted after the long modulated pulse to obtain coverage close to the radar due to the extended blind zone (Cheong et al. 2013). The surveillance and adaptive scans of the ConOps described in the previous section both cover elevations from 0.5° to 19.5° using 14 cuts, as in the volume coverage pattern (VCP) 12 used on the WSR-88D (Brown et al. 2005). For the full-size (terminal size) radar, the surveillance and initial adaptive scan times are 7.8 s (3.9 s) and 138.5 s (68.8 s), respectively. The acquisition parameters and benchmark data quality of reflectivity estimates for the lowest elevation cut (0.5°) in the surveillance and the adaptive scans are summarized in Table 2.

For all experiments, the reference radar is the KTLX WSR-88D instrument in Twin Lakes, Oklahoma. The input base data were obtained from the NCEI repository and correspond to 4 h of base data starting at 1900 UTC 20 May 2013 (ROC 1991). This dataset captures the life cycle of the EF5 (on the enhanced Fujita scale) tornado that affected the Oklahoma cities of Newcastle, Oklahoma City, and Moore. We selected this case because it has received significant attention (e.g., Kurdzo et al. 2015), but, more important, because it includes large variability of storm coverage and significant spatial gradients of reflectivity, resulting in nontrivial challenges for the chosen adaptive scanning algorithms. We used the same input data

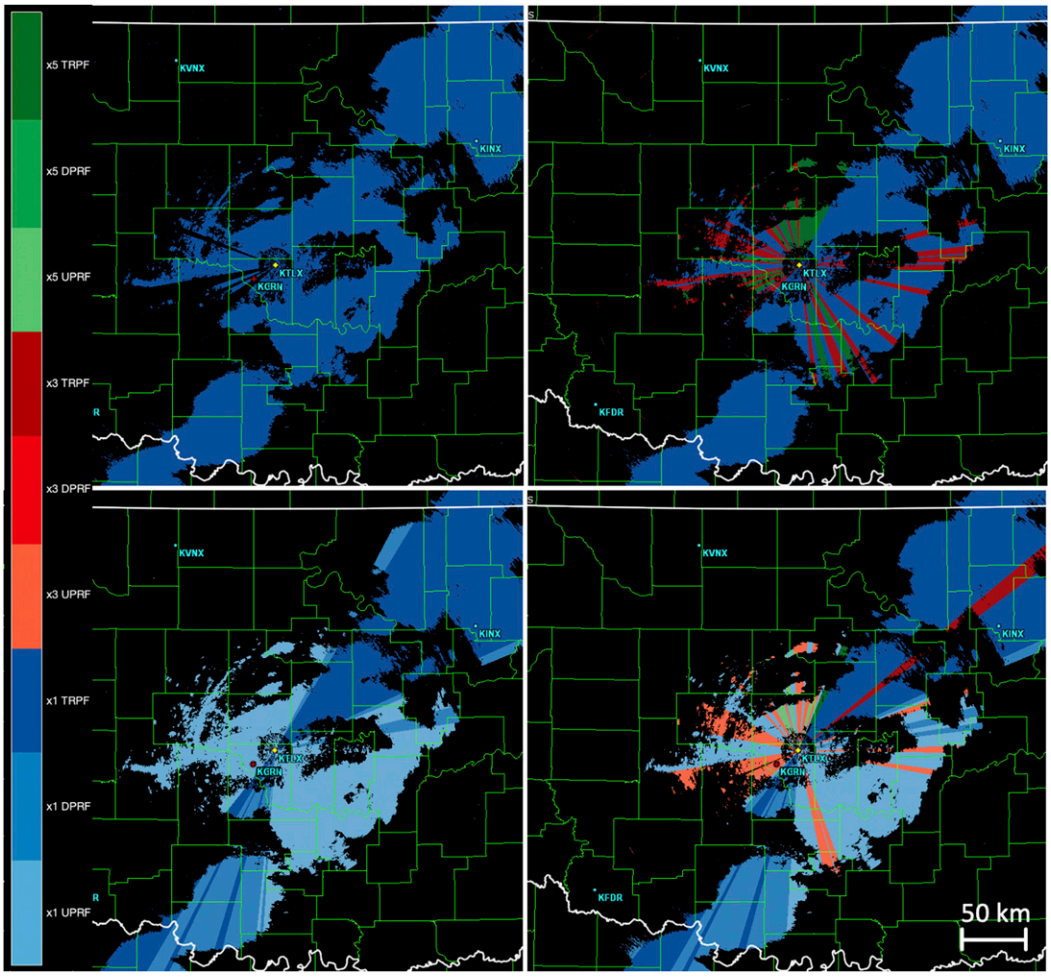

FIG. 8. As in Fig. 6, but at time B.

with both radar designs and the ConOps described in the previous section with selective application of the adaptive scanning algorithms. For the scheduler, we used a repeat count of 1 for the surveillance scan and 2 for the adaptive scan (timers were not used).

To demonstrate the flexibility of the proposed simulation framework, we consider four ConOps configurations. The first configuration consists of disabling all adaptive scanning algorithms; this is referred to as the conventional ConOps and it is used as a baseline or reference simulation. Configurations 2, 3, and 4 consist of enabling only one adaptive scanning algorithm at a time (ADAPTS, adaptive beam clustering, and adaptive dwell tailoring, respectively). Configuration 5 consists of enabling all three of the adaptive scanning algorithms concurrently. These ConOps configurations are tested on two conceptual radar designs as described above: the full-size and the terminal-size PAR. Finally, the realism of the simulated radar data is assessed through a series of experiments, where each combination of radar design and ConOps configuration is a different experiment. Experiments 1–5 use the five ConOps configurations on the full-size radar, and experiment 6 uses the fifth ConOps configuration on the terminal-size radar. For each experiment, we use the resulting simulated data to show that it can provide useful quantitative metrics. In our case, given that we chose adaptive scanning algorithms aimed at reducing the update time, we focus on measuring the resulting scan times. We also use the resulting radar data fields to confirm the realism of the simulations. For this purpose, we show that all first-order data-quality impacts predicted in section 3 are present in the simulated data. While we focus our analysis on a particular set of algorithms, ConOps, and radar designs, it should be noted that the proposed framework is flexible and not limited to these arbitrary choices. In fact, it could be used to implement and evaluate the performance of other types of adaptive scanning algorithms, ConOps, and radar designs.

Figure 3 shows the scan time for each of the four faces of the full-size radar as a function of simulation time for experiment 2 (i.e., the full-size radar using the ADAPTS algorithm). As expected, ADAPTS is very effective at reducing the scan time when the coverage of significant returns is reduced (e.g., in the presence of a few isolated storm cells). Figure 4 shows the reflectivity fields for the lowest-elevation cut (0.5°) for

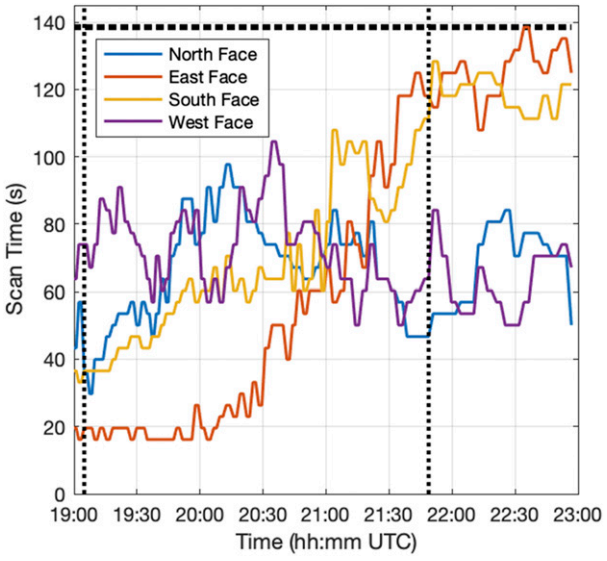

FIG. 9. As in Fig. 3, but for experiment 3 (using the adaptive beam clustering algorithm).

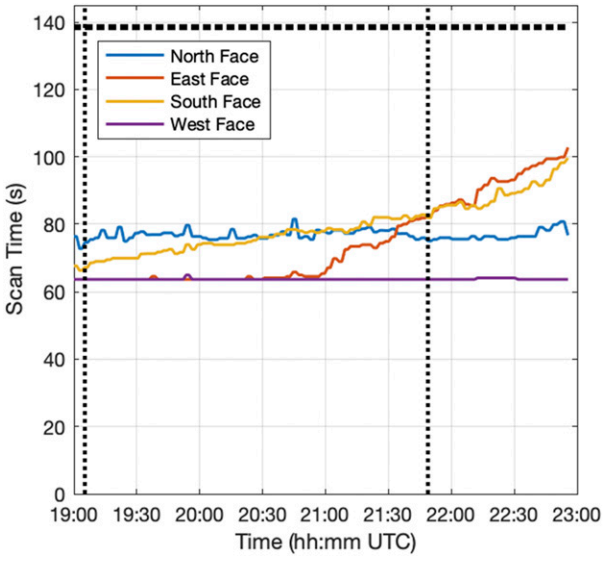

FIG. 10. As in Fig. 3, but for experiment 4 (using the adaptive dwell tailoring algorithm).

experiment 1 (full-size radar with conventional scanning) and two representative simulation times: time A (1905 UTC) corresponds to a low-coverage situation and time B (2149 UTC) to a high-coverage situation. As expected with a four-face stationary PAR, the beam broadens as the radar scans toward the edge of each 90° sector, and so does the azimuthal sampling spacing, because of our choice of sine-space sampling. Nevertheless, these effects would be present whether using adaptive scanning or not. In theory, because the four faces operate independently, a temporal discontinuity could be present in the data across adjacent 90° sectors. However, to reduce computational complexity, the simulation was configured to assume no storm evolution within the scan time, so this effect is not simulated. Figures 5–8 show reflectivity fields. The top-left panels of Figs. 5 and 7 show the reflectivity fields obtained with experiment 2 for the same two times. For time A, the use of ADAPTS resulted in time savings of 23%, where the time savings is computed using the longest scan time among all four faces and with respect to the scan time obtained with the conventional ConOps. For time B, ADAPTS did not provide any time savings because all but the west face had to cover full 90° sectors. The corresponding adaptive scanning products are also included for times A and B in the top-left panels of Figs. 6 and 8, where the beam positions enabled by ADAPTS are painted blue and the disabled ones are not painted. Comparison of Fig. 4 with the top-left panels of Figs. 5 and 7 demonstrates that, as designed, the beam positions that ADAPTS disabled do not contain significant returns. For example, all storm cells present at time A to the southwest and to the northeast of the radar can be seen in the reflectivity field obtained with ADAPTS. Significant returns to the west of the radar are also preserved, and only the weakest returns are not sampled. It can certainly be argued whether the regions not sampled by ADAPTS in this example contain useful or significant returns based on other criteria. However, the goal here is to illustrate how the proposed simulation framework can be used to evaluate, understand, and fine-tune the performance of ADAPTS.

Figure 9 is the same as Fig. 3 but for experiment 3 (i.e., the full-size radar using the adaptive beam clustering algorithm). This algorithm is more effective at reducing the scan time when the azimuthal reflectivity gradients are small. The top-right panels of Figs. 5 and 7 show the reflectivity fields for the lowest elevation cut for experiment 3 and the same times A and B identified in the previous experiment, respectively. For time A, the use of the adaptive beam clustering algorithm resulted in

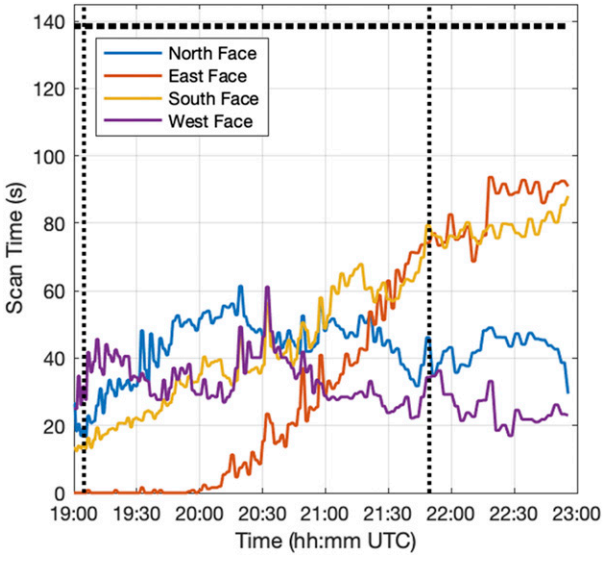

FIG. 11. As in Fig. 3, but for experiment 5 (using all three adaptive scanning algorithms concurrently).

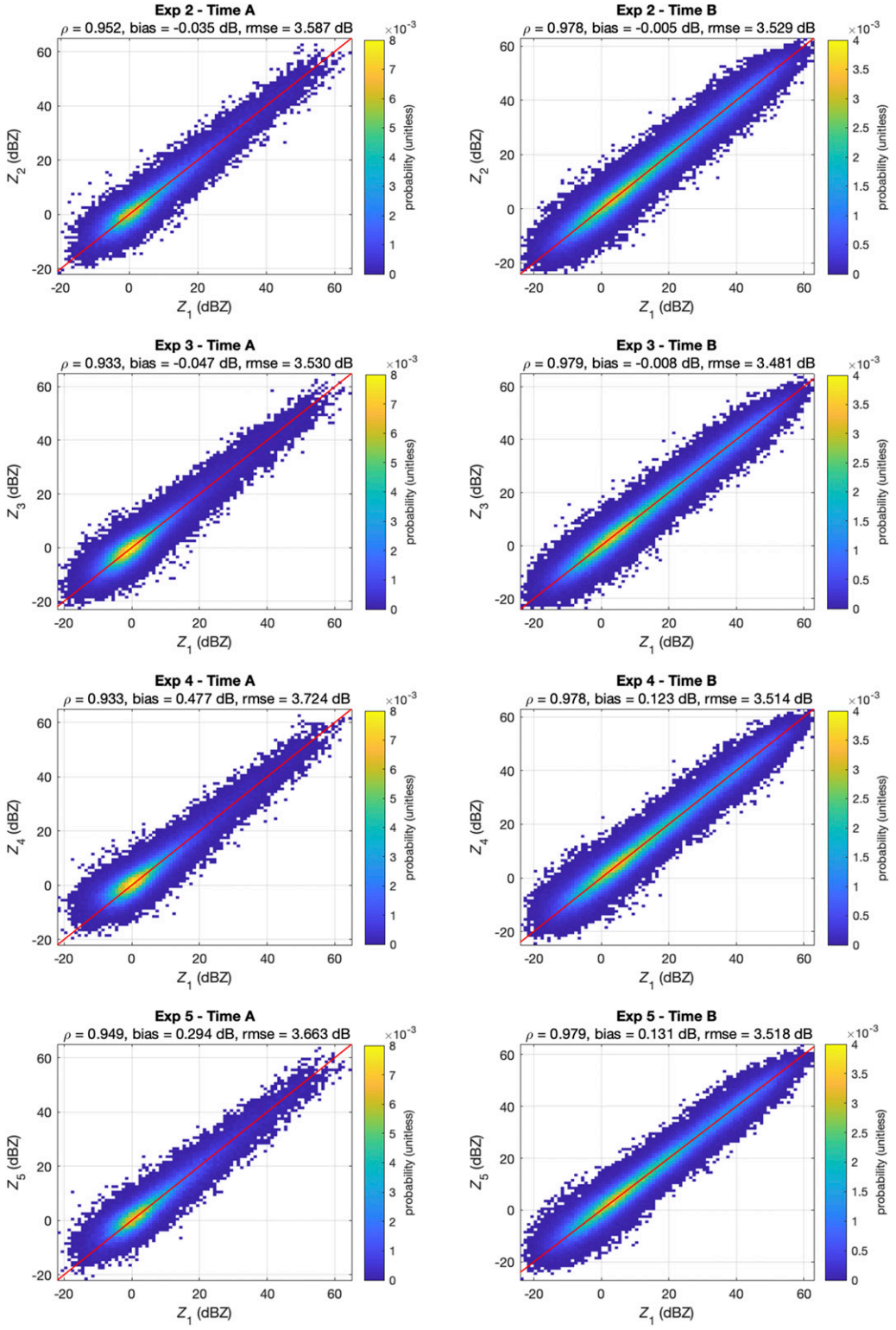

FIG. 12. Probability of reflectivity pairs for times (left) A and (right) B, where the first component (x axis) comes from experiment 1 and the second component (y axis) comes from experiments (top) 2, (top middle) 3, (bottom middle) 4, and (bottom) 5. Both components of a pair come from the same location in the reflectivity fields. The probability is computed as the ratio of the number of pairs in each 0.1 by 0.1 dBZ bin to the total number of pairs. The solid red lines are the one-to-one lines. The Pearson correlation coefficient ρ, bias, and root-mean-square error (rmse) are included for each case.

time savings of 47%. For time B, the time savings was only 15%. In this case, the adaptive scanning products in the top-right panels of Figs. 6 and 8 indicate the size of the cluster: pencil beams are painted blue, spoiled beams with a factor of 3 are painted red, and spoiled beams with a factor of 5 are painted green. Note that for the adaptive scan defined above that uses 50% overlapped beams in azimuth, spoil factors of 3 and 5 correspond to receive beam clusters of five and nine beams, respectively. Comparison of Fig. 4 and the top-right panels of Figs. 5 and 7 demonstrates that the largest beam clusters are placed in regions with no significant echoes or with more uniform reflectivity fields whereas pencil beams are placed in regions with large azimuthal reflectivity gradients. For example, at time A, beam clusters with five and nine beams are used everywhere except in the southwest sector containing a few isolated storm cells. In this sector, pencil beams are used to preserve the spatial structure of the fields. Everywhere else, the use of spoiled transmit beams does not result in obvious data-quality impacts, confirming the expected performance of the bias-limiting criterion of the adaptive beam clustering algorithm. The expected change in sensitivity from the use of spoiled transmit beams is also apparent in the coverage of simulated fields, this is especially evident in the northeast sector, where alternating transmit beams with spoil factors of 3 and 5 create spoke-like artifacts in the data. At time B, when severe storms exhibit greater coverage, the algorithm uses mostly pencil beams, with a few occurrences of five-beam clusters and even fewer of nine-beam clusters.

Figure 10 is the same as Fig. 3 but for experiment 4 (i.e., the full-size radar using the adaptive dwell tailoring algorithm). This algorithm is more effective at reducing the scan time when all storms are closer to the radar. The bottom-left panels of Figs. 5 and 7 show the reflectivity fields for the lowest elevation cut for experiment 4 and times A and B. For time A, the use of the adaptive dwell tailoring algorithm resulted in time savings of 46%. For time B, the time savings was slightly less at 41%. In this case, the adaptive scanning products in the bottom-left panels of Figs. 6 and 8 indicate the dwell type: beams with single, dual, and triple-PRF dwells are painted light, medium, and dark blue, respectively. Comparison of Fig. 4 and the bottom-left panels of Figs. 5 and 7 corroborates that the use of single- and dual-PRF dwells (instead of the initial triple-PRF ones) does not result in any loss of coverage or data quality. For example, at time A, the adaptive dwell tailoring algorithm uses single-PRF dwells almost everywhere, except in small sectors to the southwest and to the north-northeast of the radar, where the maximum range of storms is the largest. At time B, there are more beams using multi-PRF dwells, which are needed to deal with the presence of larger storms at longer ranges. Also, comparing the reflectivity fields with those in Fig. 4, we see no appreciable change in data quality. This is because reflectivity is estimated using data from the available CPI with the lowest PRF, and the adaptive algorithm adjusts the dwell times to produce data with similar quality regardless of the number of CPIs in the dwell.

Figure 11 is the same as Fig. 3 but for experiment 5 (i.e., the full-size radar using all adaptive scanning algorithms concurrently). The adaptive scanning products from each algorithm

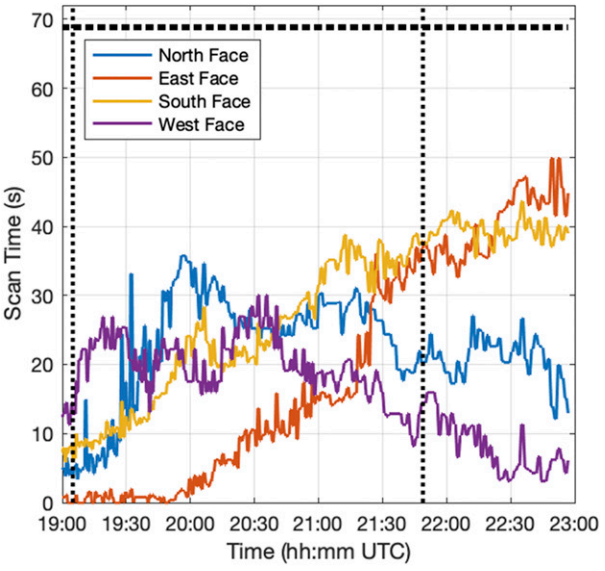

FIG. 13. As in Fig. 11, but for the terminal-size radar.

are combined using the following logic. For each cluster determined by the adaptive beam clustering algorithm, we use the ADAPTS and dwell-type outputs for the receive beams within the cluster. Only if all receive beams in a cluster were disabled by ADAPTS, the cluster is disabled. In this case, the outputs from the adaptive dwell tailoring algorithm are ignored. Otherwise, if at least one receive beam in the cluster was left enabled by ADAPTS, the entire cluster is enabled and the dwell type with the largest number of CPIs is selected. In comparing Figs. 3 and 9–11, we confirm that the fastest updates are achieved when all the available adaptive scanning algorithms are in use. The bottom-right panels of Figs. 5 and 7 show the reflectivity fields for the lowest elevation cut for times A and B. For time A, the use of all adaptive algorithms resulted in time savings of 77% (as compared with 23%, 47%, and 46% obtained while using each of the adaptive scanning algorithms individually). For time B, the time savings was 43% (as compared with 0%, 15%, and 41% obtained while using each of the adaptive scanning algorithms individually). In this case, the adaptive scanning products in the bottom-right panels of Figs. 6 and 8 indicate the resulting combination of individual adaptive scanning products.

To confirm that the simulated data exhibit the desired realism in terms of data quality, we compare the simulated reflectivity fields at times A and B from experiments 2–5 to those from experiment 1. Figure 12 shows the probability of reflectivity pairs, where the first component (x axis) comes from experiment 1 and the second component (y axis) comes from experiments 2–5 (the rows from top to bottom). Both components of a pair come from the same location in the reflectivity fields, and the probability is computed as the ratio of the number of pairs in each 0.1 by 0.1 dBZ bin to the total number of pairs. As expected, for all cases, there is a higher concentration of pairs near the one-to-one line with Pearson correlations above 0.93. There is slightly better correlation at

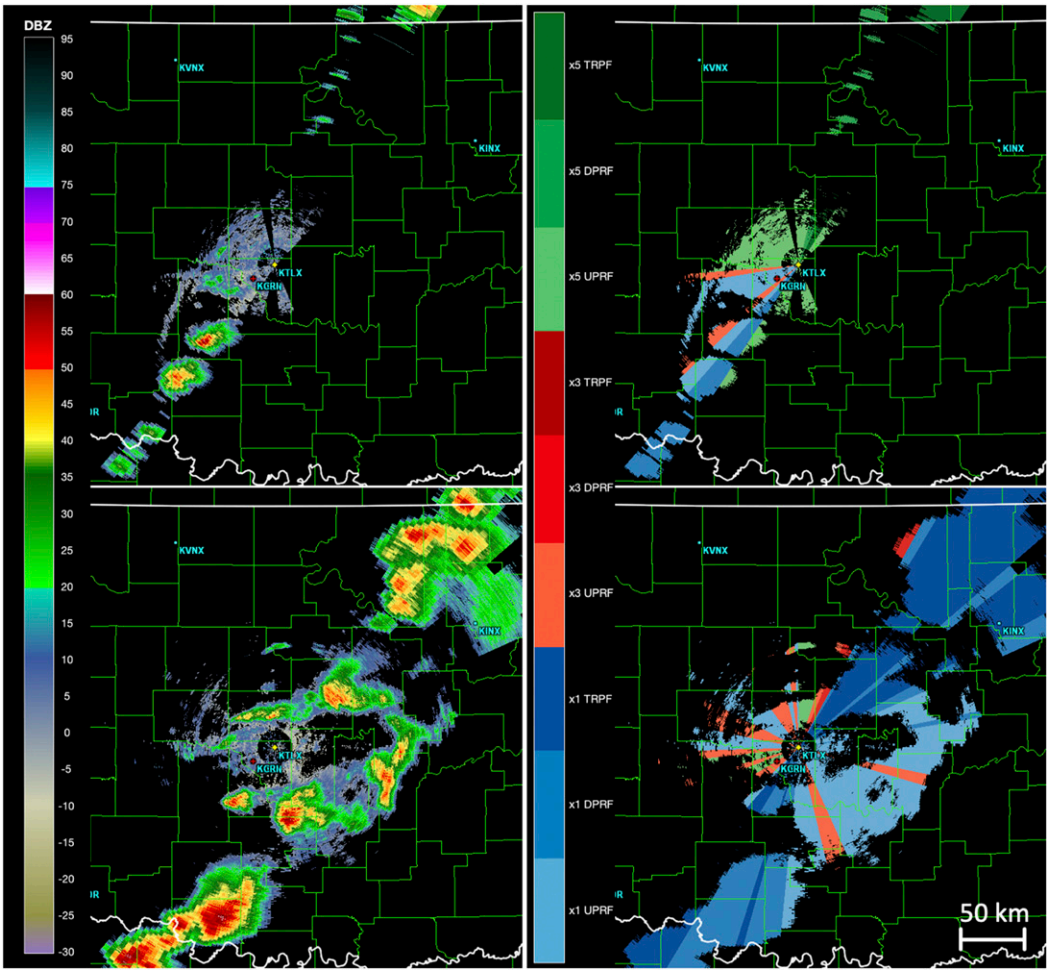

FIG. 14. (left) Fields of reflectivity and (right) corresponding adaptive scanning products for the lowest-elevation cut (0.5°) for experiment 6 (using all adaptive scanning algorithms concurrently on the terminal-size radar) for times (top) A and (bottom) B.

time B due to the larger coverage and strength of storms. The dispersion around the one-to-one line [quantified by the root-mean-square error (rmse)] is similar for all cases as it comes from expected statistical fluctuations inherent to the IQ data simulation process, which is repeated for each experiment. As expected, the biases for experiments 2 and 3 are small since neither ADAPTS or the adaptive dwell tailoring algorithm should impact the bias or standard deviation of the reflectivity data. However, the biases for experiments 4 and 5, which include the adaptive beam clustering algorithm, are meaningfully higher. This is also expected, since the use of spoiled transmit beams introduces reflectivity biases in the presence of gradients, which the adaptive scanning algorithm tries to contain. These quantitative comparisons confirm the qualitative analyses above.

Figure 13 is the same as Fig. 11 but for experiment 6 (i.e., the terminal-size radar using all adaptive scanning algorithms concurrently). Because this radar has a smaller aperture (i.e., wider beamwidths), it can cover each 90° sector with fewer transmit beams in sine space (e.g., 81 beams using 50% azimuthally overlapped pencil beams) compared to the full-size radar (e.g., 163 beams using 50% azimuthally overlapped pencil beams). Because of this, the scan times with the terminal-size radar are generally shorter than those with the full-size radar. This, of course, comes at the price of degraded sensitivity and spatial resolution. For time A, the use of all adaptive algorithms with the terminal-size radar resulted in time savings of 81% (as compared with 77% with the full-size radar); for time B, the savings is 45% (as compared with 43%). Figure 14 shows the reflectivity fields for the lowest elevation cut for experiment 6 and the same times A and B identified in previous experiments. The data-quality impacts of using a different radar are evident in the simulated radar data. Relative to the bottom-right panels of Figs. 5 and 7, the reflectivity fields in Fig. 14 exhibit degradation in azimuthal resolution (evident as a coarser structure of echoes) and reduced sensitivity (evident as smaller footprints of storms). However, while not exactly the same, the scan modifications made by the adaptive scanning algorithms are similar on both radars when sampling the same scene.

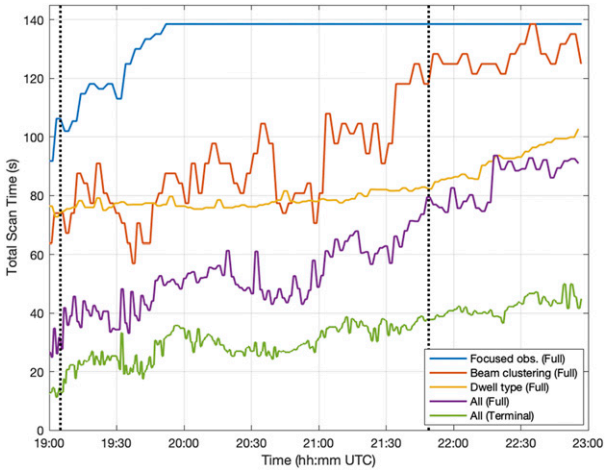

FIG. 15. Total scan time as a function of simulation time for experiments 2–6. The vertical black dotted lines correspond to time A and time B.

Figure 15 shows a comparison of total scan times for experiments 2–6, where the total scan time is obtained as the maximum scan time among all four faces. The results in this figure confirm that, for this event and using the full-size radar, ADAPTS results in the smallest time savings, generally followed by the adaptive beam clustering and the adaptive dwell type algorithms. It is also evident that the combination of all adaptive scanning algorithms leads to the shortest total scan times. As argued before, the scan times with the terminal-size radar are shorter due the fewer number of beams needed for full coverage, but the time savings as a percentage of the scan time using a conventional ConOps are similar between the two radars.

5. Conclusions

We presented a simulation framework to evaluate the performance of adaptive scanning ConOps using different phased-array radar designs. In essence, the proposed simulation framework produces realistic radar data to support the development and evaluation of feasible adaptive scanning ConOps to meet evolutionary NWS observing needs. That is, it enables the concept of the ''meteorologist in the loop'' as described by Nai et al. (2020). The simulation framework consists of three main subsystems: signal simulation, signal processing, and radar control providing sufficient flexibility and customization to simulate a variety of relevant radar designs and adaptive scanning ConOps via a modularized design. A fundamental piece of the simulator is the scan definition, which contains adaptable information that controls key aspects of radar transmission, reception, and signal processing. The simulation is driven by simple configuration files that define the main characteristics of the reference and emulated radars, including antenna geometry, transmit and receive parameters, and temporal and spatial sampling parameters.

Our experimental results used input data from a significant weather event collected by the KTLX radar and produced output data as would be observed by two different radar systems using four different ConOps configurations. These results were presented only to illustrate the flexibility of the proposed framework. Whereas comprehensive analyses of different adaptive scanning algorithms and ConOps are left for future research, the results presented here confirm that the output data produced by the simulator exhibit sufficient realism and could be useful to obtain quantitative metrics and to perform qualitative comparisons. Once the adaptive scanning algorithms and scheduler are implemented for a particular ConOps setup, exploring the performance on other weather events is straightforward: all it takes is downloading any archived set of radar data from NCEI into a separate directory and configuring the simulator to use the input data in that directory.

As the NWS evaluates potential replacement solutions for the WSR-88D, we plan to use the proposed simulation framework to inform the design and selection of potential solutions. Achieving the best trade-off between improved capabilities, cost, and complexity is challenging, and the solution to meet demanding objective requirements may include the combination of several complementary adaptive scanning algorithms. It is expected that the NWS will also want to assess cost-performance trades between various radar architectures under consideration (e.g., planar, cylindrical, rotating, and fixed multiface) and associated scanning concepts. This simulation infrastructure can tackle any or all of these different configurations. As a critical part of the radar design process, this tool could help to bridge the gaps between radar engineers, meteorologists, NWS forecasters, and decision-makers, effectively creating a ''common language'' among all stakeholders.

Acknowledgments. The authors thank Mark Weber, Chris Curtis, and three anonymous reviewers for providing comments to improve the paper. Funding was provided by NOAA/Office of Oceanic and Atmospheric Research under NOAA–University of Oklahoma Cooperative Agreement NA11OAR4320072, U.S. Department of Commerce.

REFERENCES

Andra, D. L., E. M. Quoetone, and W. F. Bunting, 2002: Warning decision making: The relative roles of conceptual models, technology, strategy, and forecaster expertise on 3 May 1999. *Wea. Forecasting*, **17**, 559–566, https://doi.org/10.1175/1520-0434(2002)017<0559:WDMTRR>2.0.CO;2.

Boettcher, J., and F. Nai, 2020: A meteorologist embedded with engineers: Bringing NWS user perspectives to the design of future operational weather radar systems. *Proc. 30th Conf. on Weather Analysis and Forecasting*, Boston, MA, Amer. Meteor. Soc., 10A.4, https://ams.confex.com/ams/2020Annual/mediafile/Manuscript/Paper367474/AMS2020%20Extended%20Abstract%2010A.4.pdf.

Bowden, K. A., P. L. Heinselman, D. M. Kingfield, and R. P. Thomas, 2015: Impacts of phased-array radar data on forecaster performance during severe hail and wind events. *Wea. Forecasting*, **30**, 389–404, https://doi.org/10.1175/WAF-D-14-00101.1.

Brotzge, J., K. Hondle, B. Philips, L. Lemon, E. Bass, D. Rude, and D. Andra Jr., 2010: Evaluation of distributed collaborative adaptive sensing for detection of low-level circulations and implications for severe weather operations. *Wea. Forecasting*, **25**, 173–189, https://doi.org/10.1175/2009WAF2222233.1.

Brown, R. A., V. T. Wood, R. M. Steadham, R. R. Lee, B. A. Flickinger, and D. Sirmans, 2005: New WSR-88D volume coverage pattern 12: Results of field tests. *Wea. Forecasting*, **20**, 385–393, https://doi.org/10.1175/WAF848.1.

Cheong, B. L., R. Kelley, R. D. Palmer, Y. Zhang, M. Yeary, and T.-Y. Yu, 2013: PX-1000: A solid-state polarimetric X-band weather radar and time-frequency multiplexed waveform for blind range mitigation. *IEEE Trans. Instrum. Meas.*, **62**, 3064–3072, https://doi.org/10.1109/TIM.2013.2270046.

Cho, J. Y. N., 2015: Revised multifunction phased array radar (MPAR) network siting analysis. MIT Lincoln Laboratory Project Rep. ATC-425, 86 pp., https://www.ll.mit.edu/sites/default/files/publication/doc/2018-05/Cho_2015_ATC-425.pdf.

Chrisman, J. N., 2009: Automated volume scan evaluation and termination (AVSET): A simple technique to achieve faster volume scan updates for the WSR-88D. *34th Conf. on Radar Meteorology*, Williamsburg, VA, Amer. Meteor. Soc., P4.4, http://ams.confex.com/ams/pdfpapers/155324.pdf.

Crum, T. D., and R. L. Alberty, 1993: The WSR-88D and the WSR-88D Operational Support Facility. *Bull. Amer. Meteor. Soc.*, **74**, 1669–1687, https://doi.org/10.1175/1520-0477(1993)074<1669:TWATWO>2.0.CO;2.

Curtis, C. D., 2018: Weather radar time series simulation: Improving accuracy and performance. *J. Atmos. Oceanic Technol.*, **35**, 2169–2187, https://doi.org/10.1175/JTECH-D-17-0215.1.

Daniel, A. E., J. N. Chrisman, C. A. Ray, S. D. Smith, and M. W. Miller, 2014: New WSR-88D operational techniques: Responding to recent weather events. *Proc. 30th Conf. on Environmental Information Processing Technologies*, Atlanta, GA, Amer. Meteor. Soc., 5.2, https://ams.confex.com/ams/94Annual/webprogram/Paper241216.html.

Doviak, R. J., and D. S. Zrnić, 1993: *Doppler Radar and Weather Observations*. 2nd ed. Academic Press, 562 pp.

Heinselman, P. L., and S. M. Torres, 2011: High-temporal-resolution capabilities of the National Weather Radar Testbed phased-array radar. *J. Appl. Meteor. Climatol.*, **50**, 579–593, https://doi.org/10.1175/2010JAMC2588.1.

——, D. L. Priegnitz, K. L. Manross, T. M. Smith, and R. W. Adams, 2008: Rapid sampling of severe storms by the National Weather Radar Testbed phased array radar. *Wea. Forecasting*, **23**, 808–824, https://doi.org/10.1175/2008WAF2007071.1.

——, D. S. LaDue, and H. Lazrus, 2012: Exploring impacts of rapid-scan radar data on NWS warning decisions. *Wea. Forecasting*, **27**, 1031–1044, https://doi.org/10.1175/WAF-D-11-00145.1.

Isom, B., and Coauthors, 2013: The atmospheric imaging radar: Simultaneous volumetric observations using a phased array weather radar. *J. Atmos. Oceanic Technol.*, **30**, 655–675, https://doi.org/10.1175/JTECH-D-12-00063.1.

Ivić, I. R., and R. J. Doviak, 2016: Evaluation of phase coding to mitigate differential reflectivity bias in polarimetric PAR. *IEEE Trans. Geosci. Remote Sens.*, **54**, 431–451, https://doi.org/10.1109/TGRS.2015.2459047.

——, C. Curtis, and S. M. Torres, 2013: Radial-based noise power estimation for weather radars. *J. Atmos. Oceanic Technol.*, **30**, 2737–2753, https://doi.org/10.1175/JTECH-D-13-00008.1.

Jeffrey, T., 2009: *Phased-Array Radar Design—Application of Radar Fundamentals*. SciTech Publishing, 341 pp.

Junyent, F., V. Chandrasekar, D. McLaughlin, E. Insanic, and N. Bharadwaj, 2010: The CASA integrated project 1 networked radar system. *J. Atmos. Oceanic Technol.*, **27**, 61–78, https://doi.org/10.1175/2009JTECHA1296.1.

Kollias, P., N. Bharadwaj, K. Widener, I. Jo, and K. Johnson, 2014: Scanning ARM cloud radars. Part I: Operational sampling strategies. *J. Atmos. Oceanic Technol.*, **31**, 569–582, https://doi.org/10.1175/JTECH-D-13-00044.1.

Kurdzo, J. M., D. J. Bodine, B. L. Cheong, and R. D. Palmer, 2015: High-temporal resolution polarimetric X-band doppler radar observations of the 20 May 2013 Moore, Oklahoma, tornado. *Mon. Wea. Rev.*, **143**, 2711–2735, https://doi.org/10.1175/MWR-D-14-00357.1.

LaDue, D. S., P. L. Heinselman, and J. F. Newman, 2010: Strengths and limitations of current radar systems for two stakeholder groups in the Southern Plains. *Bull. Amer. Meteor. Soc.*, **91**, 899–910, https://doi.org/10.1175/2009BAMS2830.1.

Lai, K. H., I. D. Longstaff, and G. D. Callahan, 2004: Super-fast scanning technique for phased array weather radar application. *Proc. Inst. Elect. Eng. Radar Sonar Navig.*, **151**, 271–279, https://doi.org/10.1049/ip-rsn:20040559.

McLaughlin, D., and Coauthors, 2009: Short-wavelength technology and the potential for distributed networks of small radar systems. *Bull. Amer. Meteor. Soc.*, **90**, 1797–1818, https://doi.org/10.1175/2009BAMS2507.1.

Meischner, P., C. Collier, A. Illingworth, J. Joss, and W. Randeu, 1997: Advanced weather radar systems in Europe: The COST 75 action. *Bull. Amer. Meteor. Soc.*, **78**, 1411–1430, https://doi.org/10.1175/1520-0477(1997)078<1411:AWRSIE>2.0.CO;2.

Melnikov, V. M., R. J. Doviak, and D. S. Zrnić, 2015: A method to increase the scanning rate of phased-array weather radar. *IEEE Trans. Geosci. Remote Sens.*, **53**, 5634–5643, https://doi.org/10.1109/TGRS.2015.2426704.

Meyer, S., O. Wang, H. Zimmer, M. Grosse, and A. Sorkine-Hornung, 2015: Phase-based frame interpolation for video. *2015 IEEE Conf. on Computer Vision and Pattern Recognition*, Boston, MA, IEEE, 1410–1418, https://doi.org/10.1109/CVPR.2015.7298747.

Nai, F., J. Boettcher, C. Curtis, D. Schvartzman, and S. Torres, 2020: The impact of elevation sidelobe contamination on radar data quality for operational interpretation. *J. Appl. Meteor. Climatol.*, **59**, 707–724, https://doi.org/10.1175/JAMC-D-19-0092.1.

Nguyen, C. M., and V. Chandrasekar, 2017: Electronic scan strategy for phased array weather radar using a space–time characterization model. *J. Atmos. Oceanic Technol.*, **34**, 921–938, https://doi.org/10.1175/JTECH-D-16-0021.1.

NWS, 2015: Radar functional requirements. NOAA Internal Rep., 58 pp., https://www.roc.noaa.gov/WSR88D/PublicDocs/NOAA_Radar_Functional_Requirements_Final_Sept%202015.pdf.

——, 2020: Weather radar follow on plan: Research and risk reduction to inform acquisition decisions. NOAA Rep., 21 pp., https://www.nssl.noaa.gov/publications/mpar_reports/RadarFollowOnPlan_ReporttoCongress_2020June_Final.pdf.

Proud, J. L., K. K. Droegemeier, V. T. Wood, and R. A. Brown, 2009: Sampling strategies for tornado and mesocyclone detection using dynamically adaptive Doppler radars: A simulation study. *J. Atmos. Oceanic Technol.*, **26**, 492–507, https://doi.org/10.1175/2008JTECHA1087.1.

Reinoso-Rondinel, R., T. Yu, and S. Torres, 2010: Multifunction phased-array radar: Time balance scheduler for adaptive weather sensing. *J. Atmos. Oceanic Technol.*, **27**, 1854–1867, https://doi.org/10.1175/2010JTECHA1420.1.

ROC, 1991: NOAA Next Generation Radar (NEXRAD) level 2 base data. NOAA National Centers for Environmental Information, accessed 26 March 2020, https://doi.org/10.7289/V5W9574V.

——, 2007: WSR-88D system specification. WSR-88D Radar Operations Center Rep. OWY55, 164 pp.

——, 2018: NEXRAD/WSR-88D history. ROC Doc., 12 pp., https://www.roc.noaa.gov/WSR88D/PublicDocs/NEXRAD.pdf.

——, 2020: WSR-88D Service Life Extension Program (SLEP). Accessed 15 April 2020, https://www.roc.noaa.gov/WSR88D/SLEP/SLEP.aspx.

Sachidananda, M., and D. S. Zrnić, 1999: Systematic phase codes for resolving range overlaid signals in a Doppler weather radar. *J. Atmos. Oceanic Technol.*, **16**, 1351–1363, https://doi.org/10.1175/1520-0426(1999)016<1351:SPCFRR>2.0.CO;2.

Schvartzman, D., and C. D. Curtis, 2019: Signal Processing and Radar Characteristics (SPARC) simulator: A flexible dual-polarization weather-radar signal simulation framework based on preexisting radar-variable data. *IEEE J. Sel. Top. Appl. Earth Obs. Remote Sens.*, **12**, 135–150, https://doi.org/10.1109/JSTARS.2018.2885614.

——, S. Torres, and T. Yu, 2017: Weather radar spatiotemporal saliency: A first look at an information theory–based human attention model adapted to reflectivity images. *J. Atmos. Oceanic Technol.*, **34**, 137–152, https://doi.org/10.1175/JTECH-D-16-0092.1.

Torres, S. M., and D. Warde, 2014: Ground clutter mitigation for weather radars using the autocorrelation spectral density. *J. Atmos. Oceanic Technol.*, **31**, 2049–2066, https://doi.org/10.1175/JTECH-D-13-00117.1.

——, and Coauthors, 2016: Adaptive-weather-surveillance and multifunction capabilities of the National Weather Radar Testbed phased array radar. *Proc. IEEE*, **104**, 660–672, https://doi.org/10.1109/JPROC.2015.2484288.

Weber, M. E., J. Y. N. Cho, J. S. Herd, J. M. Flavin, W. E. Benner, and G. S. Torok, 2007: The next-generation multimission U.S. surveillance radar network. *Bull. Amer. Meteor. Soc.*, **88**, 1739–1752, https://doi.org/10.1175/BAMS-88-11-1739.

——, ——, and H. G. Thomas, 2017: Command and control for multifunction phased array radar. *IEEE Trans. Geosci. Remote Sens.*, **55**, 5899–5912, https://doi.org/10.1109/TGRS.2017.2716935.

Yu, T.-Y., M. B. Orescanin, C. D. Curtis, D. S. Zrnić, and D. E. Forsyth, 2007: Beam multiplexing using the phased-array weather radar. *J. Atmos. Oceanic Technol.*, **24**, 616–626, https://doi.org/10.1175/JTECH2052.1.

Zrnić, D. S., and Coauthors, 2007: Agile-beam phased array radar for weather observations. *Bull. Amer. Meteor. Soc.*, **88**, 1753–1766, https://doi.org/10.1175/BAMS-88-11-1753.

——, V. M. Melnikov, R. J. Doviak, and R. Palmer, 2015: Scanning strategy for the multifunction phased-array radar to satisfy aviation and meteorological needs. *IEEE Geosci. Remote Sens. Lett.*, **12**, 1204–1208, https://doi.org/10.1109/LGRS.2014.2388202.